Proceedings of the ASME 2023 18th International Manufacturing Science and Engineering Conference
MSEC2023
June 12-16, 2023, New Brunswick, New Jersey

MSEC2023-104233

CONTROLLING RHEOLOGICAL PROPERTIES OF HYBRID HYDROGEL USING SHORT FIBER FOR EXTRUSION-BASED 3D BIOPRINTING PROCESS

Slesha Tuladhar
Department of Sustainable Product Design and Architecture, Keene State College, Keene, NH.

Scott Clark
Department of Sustainable Product Design and Architecture, Keene State College, Keene, NH.

MD Ahasan Habib*
Department of Sustainable Product Design and Architecture, Keene State College, Keene, NH.

ABSTRACT

Among various available 3D bioprinting techniques, extrusion-based three-dimensional (3D) bio-printing allows the deposition of cell-laden bio-ink, ensuring predefined scaffold architecture that may offer living tissue regeneration. With a combination of unique characteristics such as biocompatibility, less cell toxicity, and high-water content, natural hydrogels are a great candidate for bio-ink formulation for the extrusion-based 3D bioprinting process. However, due to its low mechanical integrity, hydrogel faces a common challenge in maintaining structural ty. To tackle this challenge, we characterized the rheological properties of a set of hybrid hydrogels composed of cellulose-derived nanofiber (TEMPO-mediated nano-fibrillated cellulose, TONFC), carboxymethyl cellulose (CMC) and commonly used alginate. A total of 46 compositions were prepared using higher (0.5% and 1.0%) and lower percentages (0.005% and 0.01%) of TONFC, 1%-4% of CMC, and 1%-4% of alginate to analyze the rheological properties. The shear thinning coefficients of n and K were determined for each composition from the flow diagram and co-related with the 3D printability. The ability to control rheological properties with various ratios of a nanofiber can help achieve a 3D bio-printed scaffold with defined scaffold architecture.

1. INTRODUCTION

A new technology called three-dimensional (3D) bioprinting uses scaffolding and carefully regulated cell and biomaterial distribution to replicate biological tissues. The bio-fabrication process is heavily researched for regenerative medicine research for a variety of application areas, including tissue engineering, transplantation and clinics, pharmaceutics, high-throughput screening, and cancer research [1-6]. This is because of its spatial and temporal deposition capability through the fabrication parameters. The most popular bio-printing modalities include inkjet [7, 8], extrusion-based [9, 10], and laser-assisted [11, 12] systems. Following a vectorized toolpath, a variety of materials can be printed parallel to the XY plane, and the z-axis movement ensures the progressive 3D build height of the scaffold construct. The viscosity and density of the 3D bio-printable biomaterials, which are frequently referred to as bioink, must be appropriate for the printing technology. It must also be able to maintain its shape for a predetermined amount of time and must exhibit biocompatibility through good cell viability both before and after printing. Thus, three characteristics such as printability, shape integrity, and biocompatibility are necessary for the bioink to work properly [12]. Printability, shape integrity, and biocompatibility can be defined and measured with multiple characteristics such as material-wise: viscosity, pH, functional group, microstructure and process parameter-wise: printing pressure, speed, nozzle diameter, print distance, temperature [13].

Because it is simple to prepare and has regulated rheological behavior, naturally derived sodium alginate is one of the hydrogel materials that is frequently utilized in extrusion bio-printing [14]. Even higher weight percentage and higher molecular weight can increase the viscosity of materials, higher viscosity may jam the dispensing nozzle, requiring additional force to clear it, distorting the print and lowering cell viability [4]. Due to low modulus, it is also difficult to achieve well-defined 3D shape, size, and dimensional integrity after printing. The deposited filament must possess sufficient mechanical strength to support the ensuing layers [1]. Making large-scale scaffolds also requires maintaining the shape accuracy of the scaffold, which requires little dispersion and filament sagging after printing [2]. Carboxymethyl cellulose (CMC) is a polysaccharide and cellulose derivative. It is used to change viscosity, has a large molecular weight, and is soluble in water [15]. Additionally, the binding of the CMC's matrix protein aids in cell adhesion and movement [16]. To obtain improved physical and mechanical qualities, several researchers have mixed CMC with alginate. To enhance the mechanical and biological (for example, cell development) capabilities of the base hydrogel material, nano-scale reinforcements such as polylactic acid (PLA) nanofibers and nano-fibrillated cellulose (NFC) have been studied [17, 18]. However, because to the unpredictable nature of the pressure need and the non-uniformity of network entanglements in the pure NFC gel, it was extremely challenging to 3D print them [19]. The surface of the NFC-based gel is altered by oxidation using 2,2,6,6 tetramethyl-1-

piperidinyloxy (TEMPO) to add negatively charged carboxylate ions, which is known as TO-NFC, to improve uniformity, dispersibility, homogeneity, and printability (TempO-NFC).
In our earlier research, we developed a novel bio-ink comprised with alginate, carboxymethyl cellulose (CMC), and TEMPO-mediated nano-fibrillated cellulose-TONFC limiting the solid content 5% (2% alginate, 2% CMC, and 1% TONFC) that ensured fabrication of scaffold with a build height of 9.6mm and 93% cell viability [13]. As an extension of that work, we explored the effect of very low and high percentage of TO-NFC on varying percent of alginate and CMC in this paper. Extensive rheological experiments were conducted on a total of 46 compositions prepared with a varying percentage of alginate, CMC, and TO-NFC. The reduction of viscosity with increasing the shear rate, commonly known as shear thinning behavior of those compositions was analyzed and co-related with various percentages of TO-NFC. Shear thinning behavior eases the extrusion of compositions during bioprinting by reducing the viscosity and increasing the shear forces. After the release of compositions from nozzle, the shear rate drops with a corresponding rise in viscosity and an intention to preserve the shape fidelity of filament. With a higher zero-shear viscosity of any composition can contribute to preserve the shape of 3D printed filament [6].Therefore, it is important to characterize the shear thinning behavior of any composition intending for extrusion bioprinting with a wide range of shear rate starting with a small value (close to zero-shear rate). This can equally indicate the flowability during extrusion and ability to preserver shape of extruded filament. Finally, we chose some compositions having very low and high percentages of TO-NFC to 3D print filament, analyze the shape fidelity, and co-relate the result.

2. MATERIALS AND METHODS

2.1 Processing of TO-NFC and Hydrogel Preparation

Dry TEMPO nano-fibrillated cellulose (TO-NFC) $[(C_6H_{10}O_5)_x(C_6H_9O_4CO_2Na)_y]$ with a carboxylate level 0.2 to 2 mmol/g solids was acquired from the Process Development Center (PDC) at the University of Maine. Four different percentages of dry TO-NFC such as 0.005%, 0.01%, 0.5%, and 1.0% (w/v) were prepared using a magnetic stand-up stirrer with 600 rpm for 24 hours at room temperature. Various percentages of medium (viscosity ≥2000 cps of 2% in water) viscous Alginate (1, 2, 3, and 4%, w/v) and CMC (1, 2, 3, and 4%, w/v) (pH: 6.80) (Sigma-Aldrich, St. Louis, MO, USA) were mixed with prepared TO-NFC with a magnetic stand-up stirrer to make a uniform composition. Compositions used in this paper to prepare the bio-ink are shown in Table 1 where letters 'A', 'C', and 'T' represent Sodium alginate, Carboxymethyl cellulose, and tempo mediated Nano fibrillated cellulose, respectively. The numerical subscripts represent the weight percentage of the component mixed into the water to prepare the material compositions. The addition of CMC and TO-NFC will increase the overall viscosity of the material [25, 33], which will assist in achieving better printability and shape fidelity.

TABLE 1: VARIOUS COMPOSITIONS PREPARED WITH DIFFERENT WEIGHT PERCENTAGES OF ALGINATE (1, 2, 3, and 4%, w/v), CMC (1, 2, 3, and 4%, w/v), AND 0.005% (w/v), 0.5% (w/v), 0.01% (w/v), AND 1% (w/v) TO-NFC.

Alginate (A), %	CMC (C), %	TO-NFC (T), %	Symbol
1	1	x=0.005 and 0.05	$A_1C_1T_x$
	2		$A_1C_2T_x$
	3		$A_1C_3T_x$
	4		$A_1C_4T_x$
2	1		$A_2C_1T_x$
	2		$A_2C_2T_x$
	3		$A_2C_3T_x$
	4		$A_2C_4T_x$
3	1		$A_3C_1T_x$
	2		$A_3C_2T_x$
	3		$A_3C_3T_x$
4	1		$A_4C_1T_x$
	2		$A_4C_2T_x$
1	1	y=0.01 And 1.0	$A_1C_1T_y$
	2		$A_1C_2T_y$
	3		$A_1C_3T_y$
	4		$A_1C_4T_y$
2	1		$A_2C_1T_y$
	2		$A_2C_2T_y$
	3		$A_2C_3T_y$
3	1		$A_3C_1T_y$
	2		$A_3C_2T_y$
4	1		$A_4C_1T_y$

2.2 Rheological test

We conducted the rheological tests with a rotational rheometer (MCR 102, Anton Paar, Graz, Austria) having a parallel plate geometry (25.0 mm flat plate). The plate-to-plate gap was maintained at 1.0 mm, and all data were recorded at room temperature (25°C) having the intention that the extrusion process will be performed at room temperature to have a quick gelation of the deposited filament [20]. For flow curve analysis, a steady rate sweep test was conducted having a variable shear strain from 0.1 to 100 s^{-1}. We mainly focused on the flow behavior of the considered compositions. Since during extrusion, the hydrogels show the shear thinning regime across all applied shear rates (i.e., Non-Newtonian Fluids), it is appropriate to fit the viscosity values with respect to the shear rate using Ostwald–de Waele relationship or commonly known as Power Law Model [21, 22]. This Powe-Law (Equation 1) is widely used to estimate the shear thinning co-efficient of n and K for 3D bioprintable hydrogels by fitting the viscosity value with respect to the shear rate [23]:

$$\eta = K\dot{\gamma}^{n-1} \quad (1)$$

Where η is the viscoand sity, $\dot{\gamma}$ is the shear rate. While the material is extruded through the nozzle, shear stress occurs throughout the material and is larger along the nozzle wall. A nonlinear curve fitting module (Allometric) of OriginPro 2022b (Originlab, Northampton, MA, USA) was used to fit the

viscosity vs shear rate data for each composition to determine the value of n and K.

2.3 3D printing and shape fidelity analysis

We used an extrusion-based 3D bio-printer [BioX (CELLINK, Boston, MA)] to fabricate the filaments and scaffolds. We prepared hydrogels, accordingly, loaded them into a 3.0 ml disposable nozzle, and extruded pneumatically on a stationary build plane. The printing parameters we used in fabricating the scaffolds were a nozzle diameter of 450 µm, print speed of 8 mm/s, and air pressure varying from 80-170 kPa. A visual basic-based Computer-Aided Design (CAD) software, Rhino 6.0 (https://www.rhino3d.com), was used to design and define the vectorized toolpath of a scaffold. Slicer (https://www.slicer.org), a G-code generator software was used to generate a Bio-X compatible file including the toolpath coordinates and all process parameters to build the scaffold. We followed a layer-upon-layer fashion to release the materials. The images of fabricated filaments were captured using the CK Olympus bright field microscope [24]. The width of the filament is determined using ImageJ software.

2.4 Statistical analysis

We collected data following a format of "mean ± standard deviation" and analyzed them using a significance level of p = 0.05 with a two-way ANOVA. Calculations were done with n=3 unless otherwise stated. We used a statistical software, Origin Pro 2021b to analyze quantitatively and graphically.

3. RESULTS AND DISCUSSION

Rheological properties of the compositions were determined especially in terms of its viscosities. Through the Flow Curve test on all the compositions, the shear thinning behavior of the compositions were accessed. This revealed the impact of various concentration of the Nano fibers in the viscosities of different compositions portrayed in following subsections.

3.1 Flow behavior of hydrogels prepared by 0.005% and 0.5% TO-NFC

With the use of 0.005% of TO-NFC, all the compositions with varying concentrations of Alginate and CMC showed a shear thinning behavior. $A_1C_1T_{0.005}$ showed the least viscosity while $A_1C_4T_{0.005}$ and $A_2C_4T_{0.5}$ showed the highest and similar viscosities. Results are shown in Figure 1 and Figure 2. Similarly, $A_1C_1T_{0.5}$ lies at the lowest spectrum of the viscosity while $A_1C_4T_{0.5}$ showed the highest viscosity. Also, when $T_{0.005}$ and $T_{0.5}$ are compared, compositions with $T_{0.5}$ have higher viscosities than the compositions mixed with $T_{0.005}$. This concludes that higher the concentration of the TO-NFC, higher is the viscosity of the composition when the composition of Alginate and CMC are kept constant.

Figure 1 and Figure 2 demonstrate that all considered compositions show a shear thinning behavior for each applied shear rate. As mentioned in section 2.2, this phenomenon qualifies using the Power Law Model to estimate shear thinning coefficient n and k using the viscosity vs shear rate data by fitting a curve module (Allometric) for each composition. For each composition, adjusted R-square value was more than 90% implies a good fit.

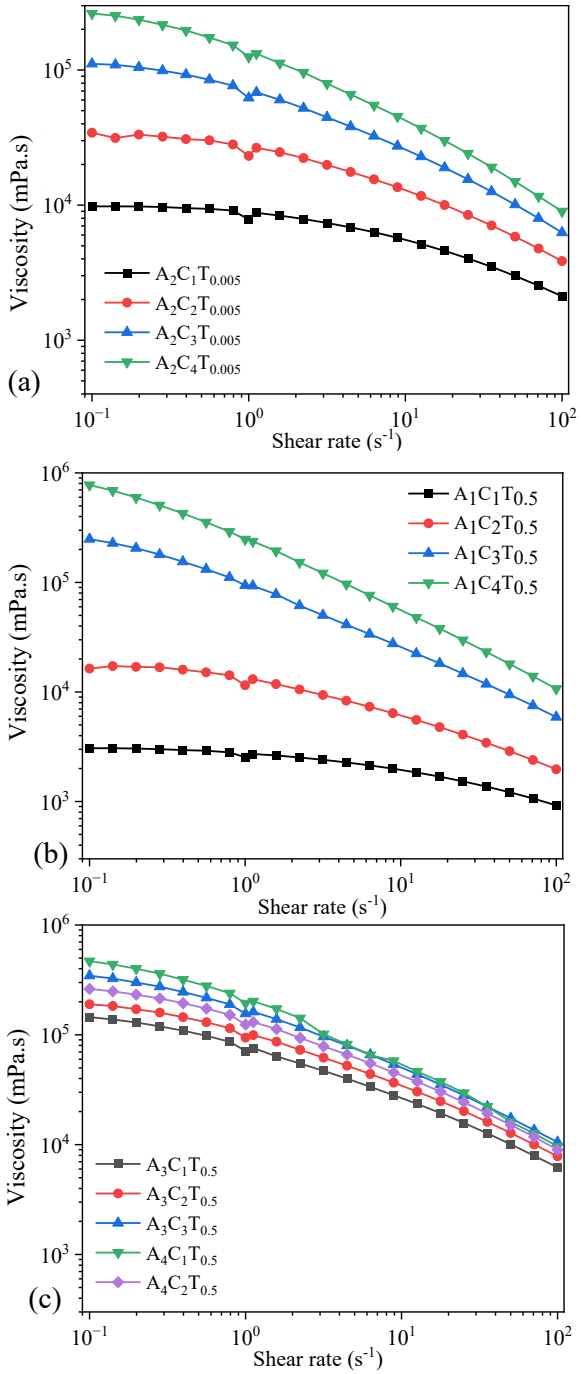

FIGURE 1: VISCOSITY OF COMPOSITIONS COMPOSED WITH VARIOUS PERCENTAGES OF ALGINATE (1-4%) AND CMC (1-4%) WITH A CONSTANT PERCENTAGE (0.005%) OF TO-NFC.

For an example, to determine the n and K values of $A_1C_4T_{0.01}$ and $A_1C_4T_1$, the fit curves are showing in Figure 3. Adjusted R-square values for the curves fitted for $A_1C_4T_{0.01}$ and $A_1C_4T_1$ compositions were 92.9% and 98.6% respectively as shown in

Figure 3. Similarly, the n and K values for all other compositions were determined in this paper. Upon the calculation of the shear thinning factors, n and k of the compositions shown in Figure 4, for all compositions we found n<1 which implies all have shear thinning behavior. The value of K increases with the increase in the concentration of TO-NFC. Figure 4 also depicts an interesting phenomenon that irrespective of percentage of TO-NFC (either 0.005% or 0.5%), the n and K values showed an inverse relation.

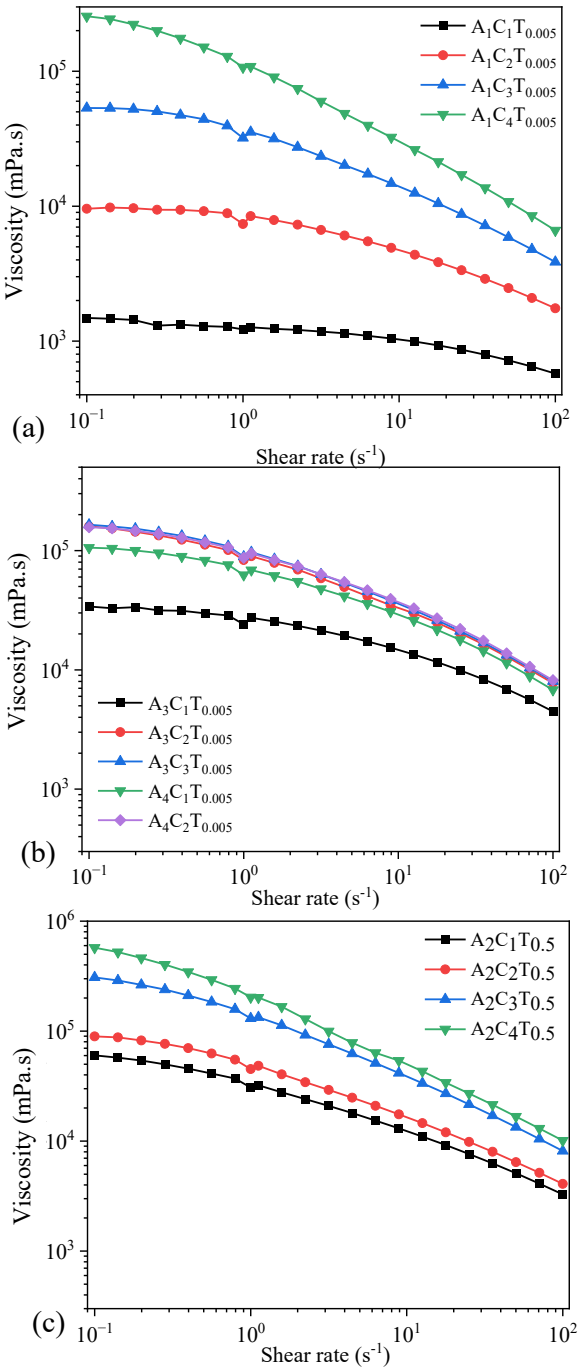

FIGURE 2: (a-c) VISCOSITY OF COMPOSITIONS COMPOSED WITH VARIOUS PERCENTAGES OF ALGINATE (1-4%) AND CMC (1-4%) WITH A CONSTANT PERCENTAGE (0.5%) OF TO-NFC.

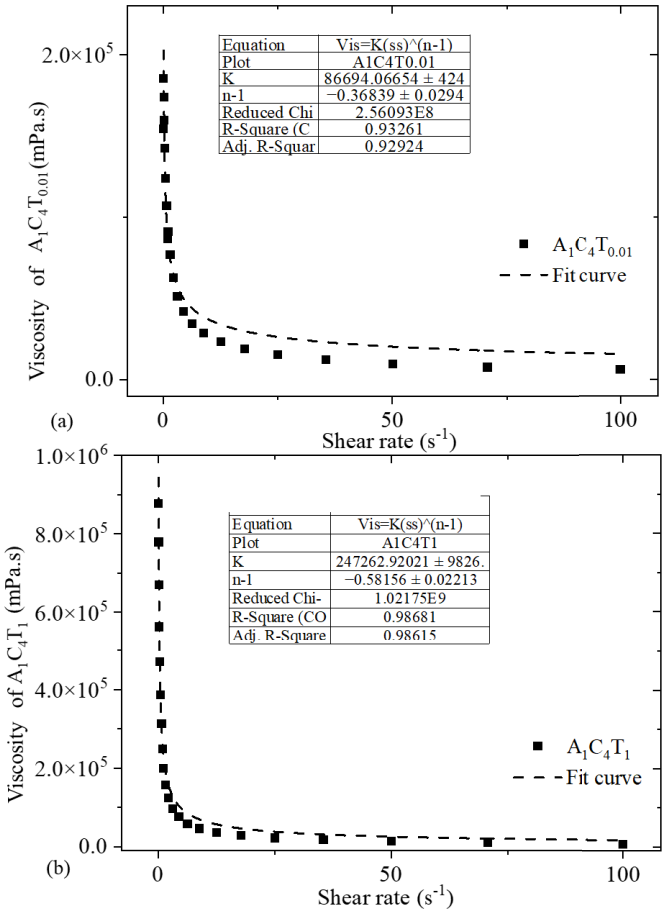

FIGURE 3: ESTIMATING THE VALUES OF SHEAR THINNING FACTORS (n AND K) OF COMPOSITIONS (a) $A_1C_4T_{0.01}$ AND (b) $A_1C_4T_1$. FOR $A_1C_4T_{0.01}$, n and K VALUES WERE 0.64 AND 86694±424 (mPa.s) WITH AN R-SQUARE VALUE OF 0.929, WHEREAS, FOR $A_1C_4T_1$, n AND K VALUES WERE 0.42 AND 247262±9826 (mPa.s) WITH AN R-SQUARE VALUE OF 0.9868.

The value of n close to 1.0 means hydrogel has the viscosity like water. Lower n value represents higher shear thinning capacity (i.e., tendency of higher viscosity reduction with small increment of the shear rate on the hydrogel). For an example, the n values for $A_1C_1T_{0.005}$ and $A_1C_1T_{0.5}$ are 0.90 and 0.86 where the K values are 1222 and 2535 mPa.s respectively as shown in Figure 4. For both compositions, the n and K values are inversely related. Either n or K values confirm that $A_1C_1T_{0.5}$ is more viscous than $A_1C_1T_{0.005}$.

The shear thinning factor K is determined at the shear rate $1.0s^{-1}$. For a comparison purpose, we will mostly use the K value throughout the paper. With a constant percentage of TO-NFC (either 0.005% or 0.5%) and alginate (either 1%, or 2%, or 3%, or 4%), the viscosity was dictated by the percentage of CMC. For an example: $A_1C_4T_{0.005}$ showed highest amount of K value

between $A_1C_1T_{0.005}$, $A_1C_2T_{0.005}$, $A_1C_3T_{0.005}$, and $A_1C_4T_{0.005}$. Similar phenomenon was observed for $A_2C_4T_{0.005}$, $A_3C_3T_{0.005}$, and $A_4C_2T_{0.005}$ as shown in Figure 1. However, for a similar percentage of solid content (i.e., summation of percentage of all components into a specific composition), CMC may not control the K value all the time. For an example, the K values for $A_1C_4T_{0.005}$, $A_2C_3T_{0.005}$, $A_3C_2T_{0.005}$, and $A_4C_1T_{0.005}$ were 106999, 62205, 83266, and 62491 mPa.s respectively. Here the summation of solid content for each composition is 5.005%. Composition ($A_1C_4T_{0.005}$) having a 4% CMC showed highest K value. From the data, it is clear that the K value did not follow a trend with the percentage of CMC.

Even with increasing the percentage of TO-NFC from 0.005% to 0.5%, a comparable scenario was also observed for the K value of $A_1C_4T_{0.5}$, $A_2C_3T_{0.5}$, $A_3C_2T_{0.5}$, and $A_4C_1T_{0.5}$ (247426, 130574, 94258, and 193857 mPa.s respectively) as shown in Figure 2. Here, the summation of solid content for each composition is 5.5% and K value was not fully governed by the percentage of CMC.

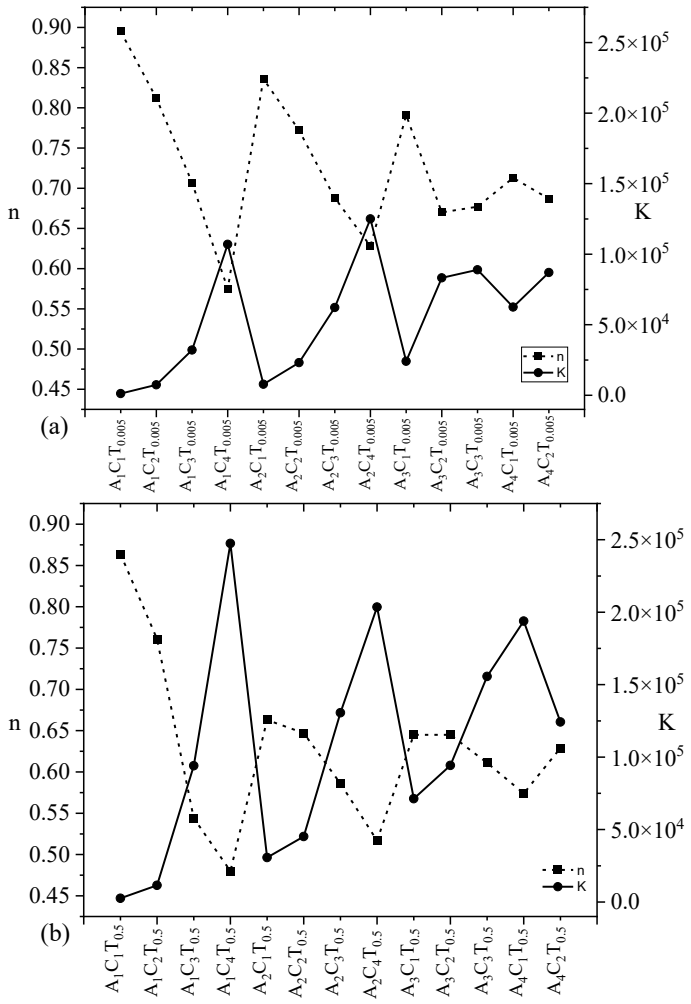

FIGURE 4: SHEAR THINNING FACTORS (n and K) OF COMPOSITIONS COMPOSED WITH VARIOUS PERCENTAGES OF ALGINATE (1-4%) AND CMC (1-4%) WITH A CONSTANT PERCENTAGE (a) 0.005% AND (b) 0.5% of TO-NFC. ALL n VALUES LESS THAN 1 CONFIRM A SHEAR-THINNING BEHAVIOR OF ALL COMPOSITIONS.

3.2 Flow behavior of hydrogels prepared by 0.01% and 1.0% TO-NFC

Now, we increased the percentage of TO-NFC from 0.005% to 0.01% and 0.5% to 1.0% to analyze the viscosity and related shear thinning factors changes. From Figure 5, $A_1C_1T_{0.01}$ showed significantly less viscosities than any of the compositions while $A_4C_1T_{0.01}$ had the highest viscosities of all. Similarly, $A_1C_1T_1$ projected the smallest viscosity while $A_1C_4T_1$ showed the highest (Figure 6). The changes in the concentration of TO-NFC had the slight impact in the viscosity of compositions as compared to when the concentrations were changed from 0.005% to 0.5%. The value of $n<1$ so they all show a shear thinning properties. The value of K within constant concentration of TONFC and alginate depicts that the viscosity heavily also depends upon the concentration of CMC which is used as a viscosity thickener.

However, as discussed earlier, for a similar percentage of solid content, CMC may not control the K value all the time. For an example, the K values for $A_1C_4T_{0.01}$, $A_2C_3T_{0.01}$, $A_3C_2T_{0.01}$, and $A_4C_1T_{0.01}$ were 86694, 53915, 48302, and 98458 mPa.s respectively. Here the summation of solid content for each composition is 5.01%. Composition ($A_1C_4T_{0.01}$) having a 4% CMC showed highest K value. Outlined data clarifies that K value did not follow a trend with the percentage of CMC. Even a similar phenomenon was observed with 1% TO-NFC leaving the percentages of alginate and CMC unchanged. The K values for $A_1C_4T_1$, $A_2C_3T_1$, $A_3C_2T_1$, and $A_4C_1T_1$ were 247785, 166808, 184119, and 424153 which did not follow any trend with the percentage of CMC.

Figure 7 follows the similar trend of Figure 4 where the n and K values showed an inverse relation irrespective of percentage of TO-NFC (either 0.01% or 1.0%), Lower n value represents tendency of higher viscosity reduction with small increment of the shear rate on the hydrogel. As a proof, the n values for $A_1C_1T_{0.01}$ and $A_1C_1T_1$ are 0.87 and 0.55 where the K values are 2034 and 14422 mPa.s respectively as shown in Figure 7. Therefore, the n and K values are inversely related for both compositions and confirm $A_1C_1T_1$ is more viscous than $A_1C_1T_{0.01}$.

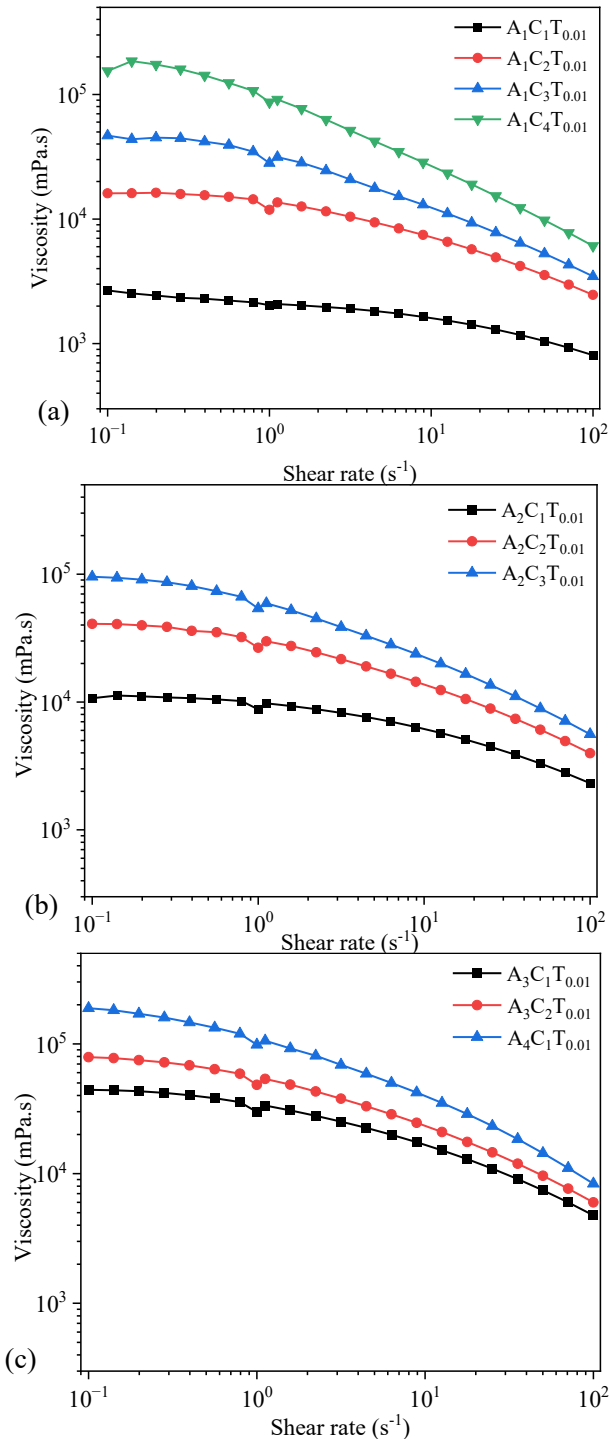

FIGURE 5: VISCOSITY OF COMPOSITIONS COMPOSED WITH VARIOUS PERCENTAGES OF ALGINATE (1-4%) AND CMC (1-4%) WITH A CONSTANT PERCENTAGE (0.01%) OF TO-NFC. ALL COMPOSITIONS SHOWED A SHEAR-THINNING BEHAVIOR.

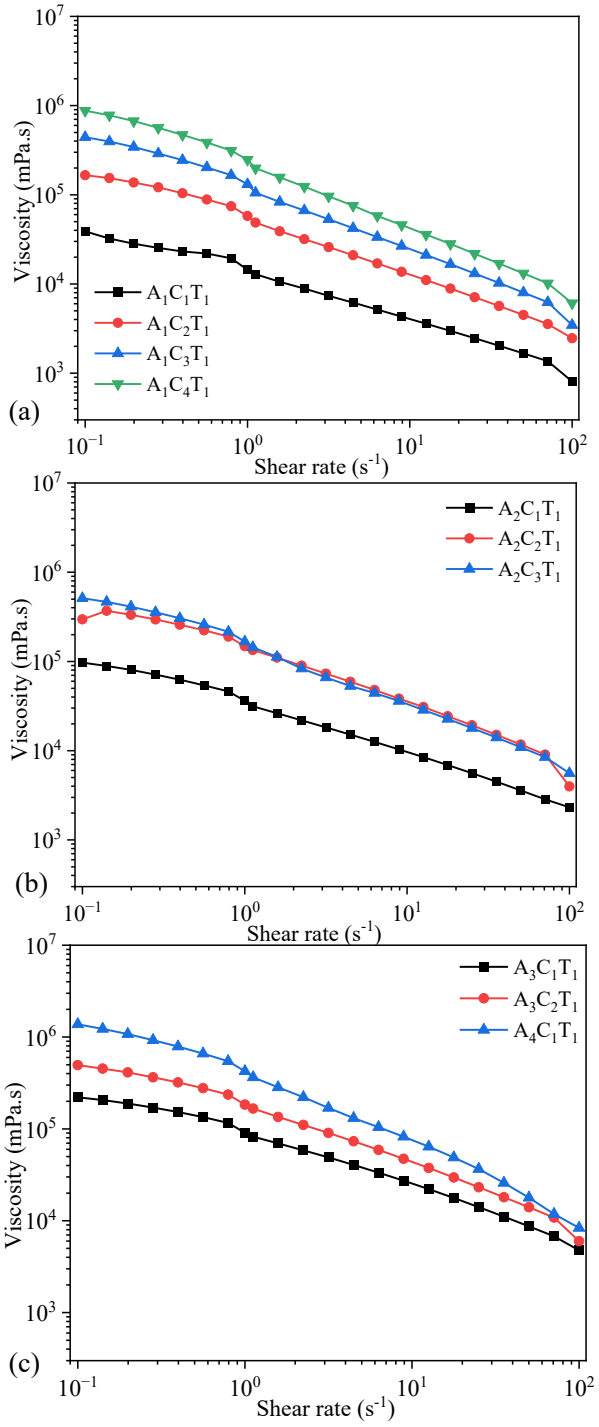

FIGURE 6: VISCOSITY OF COMPOSITIONS COMPOSED WITH VARIOUS PERCENTAGES OF ALGINATE (1-4%) AND CMC (1-4%) WITH A CONSTANT PERCENTAGE (1.0%) OF TO-NFC. ALL COMPOSITIONS SHOWED A SHEAR-THINNING BEHAVIOR.

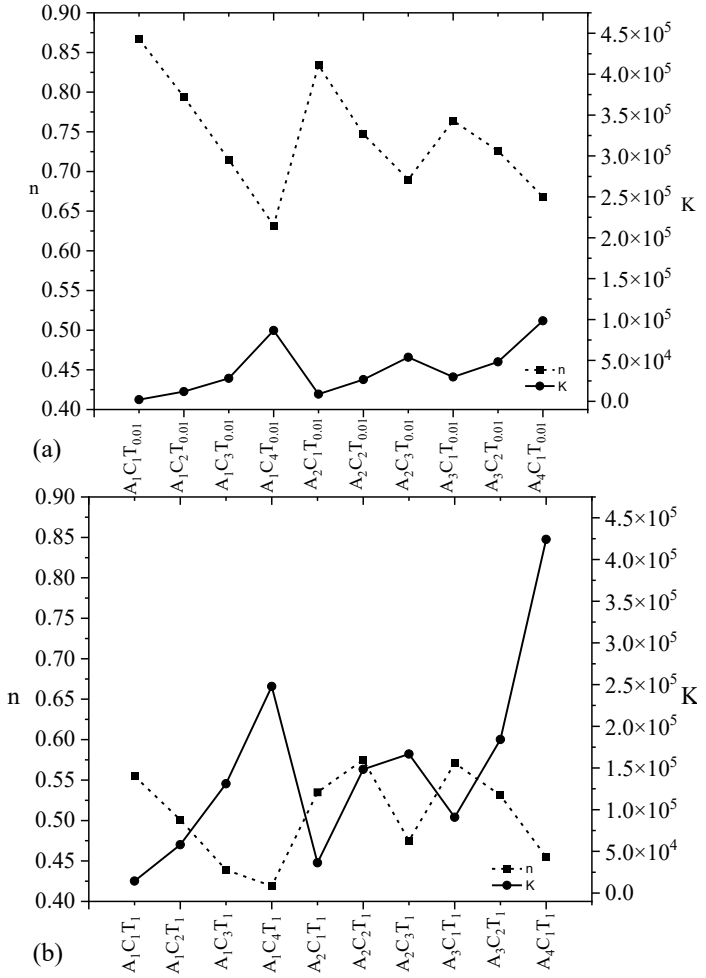

FIGURE 7: SHEAR THINNING FACTORS (n AND K) OF COMPOSITIONS COMPOSED WITH VARIOUS PERCENTAGES OF ALGINATE (1-4%) AND CMC (1-4%) WITH A CONSTANT PERCENTAGE (a) 0.01% AND (b) 1.0% OF TO-NFC. ALL n VALUES LESS THAN 1 CONFIRM A SHEAR-THINNING BEHAVIOR.

3.3 Impact of higher percentages of TO-NFC over lower percentage of TO-NFC

In this paper, we used total four different weight percent of TO-NFC such as 0.005%, 0.01%, 0.5% and 1.0% (w/v) with various percentages of alginate (1-4%) and CMC (1-4%). Two of them are at the lower end such as 0.005% and 0.01% and rest of them are at the higher end such as 0.5% and 1.0%. In both cases, we increased the TO-NFC amount 100 times such as 0.005% to 0.5% and 0.01% to 1.0% to realize the impact of it. We demonstrated the % of K increase of $A_1C_1T_1$, $A_1C_2T_1$, $A_1C_3T_1$, $A_1C_4T_1$, $A_2C_1T_1$, $A_2C_2T_1$, $A_2C_3T_1$, $A_3C_1T_1$, $A_3C_2T_1$, and $A_4C_1T_1$ with respect to the same composition of Alginate and CMC prepared with 0.01% of TO-NFC as shown in Figure 8(a). We observed a range of the percentage of K increase from 205% ($A_1C_4T_1$) to 609% ($A_1C_1T_1$) compared to the same composition of Alginate and CMC prepared with 0.01% of TO-NFC (such as $A_1C_4T_{0.01}$ and $A_1C_1T_{0.01}$). Increasing 100% TO-NFC from 0.01% to 1.0% increases the crosslinking density into each composition due to the more availability of carbonyl ion (-COO-). Moreover, the hydrogen bonds between the same carbonyl ion make the composition stronger prepared with 1.0% of TO-NFC.

We also demonstrated the similar behavior of % of K increase of $A_1C_1T_{0.5}$, $A_1C_2T_{0.5}$, $A_1C_3T_{0.5}$, $A_1C_4T_{0.5}$, $A_2C_1T_{0.5}$, $A_2C_2T_{0.5}$, $A_2C_3T_{0.5}$, $A_2C_4T_{0.5}$, $A_3C_1T_{0.5}$, $A_3C_2T_{0.5}$, $A_3C_3T_{0.5}$, $A_4C_1T_1$ and $A_4C_2T_1$ with respect to the same composition of Alginate and CMC prepared with 0.005% of TO-NFC as shown in Figure 8(a). We observed a range of the percentage of K increase from 13.2% ($A_3C_2T_{0.5}$) to 292% ($A_2C_1T_{0.5}$) compared to the same composition of Alginate and CMC prepared with 0.01% of TO-NFC (such as $A_3C_2T_{0.005}$ and $A_2C_1T_{0.005}$). Since, 1% TO-NFC provides more sites to form internal crosslink compared to 0.5% TO-NFC, we observed higher change of percentage of K increase for the compositions having 1% TO-NFC. Increasing 100% TO-NFC from 0.005% to 0.5% increases the crosslinking density into each composition due to the more availability of carbonyl ion (-COO-). The hydrogen bonds between the same carbonyl ion make the composition stronger prepared with 0.5% of TO-NFC.

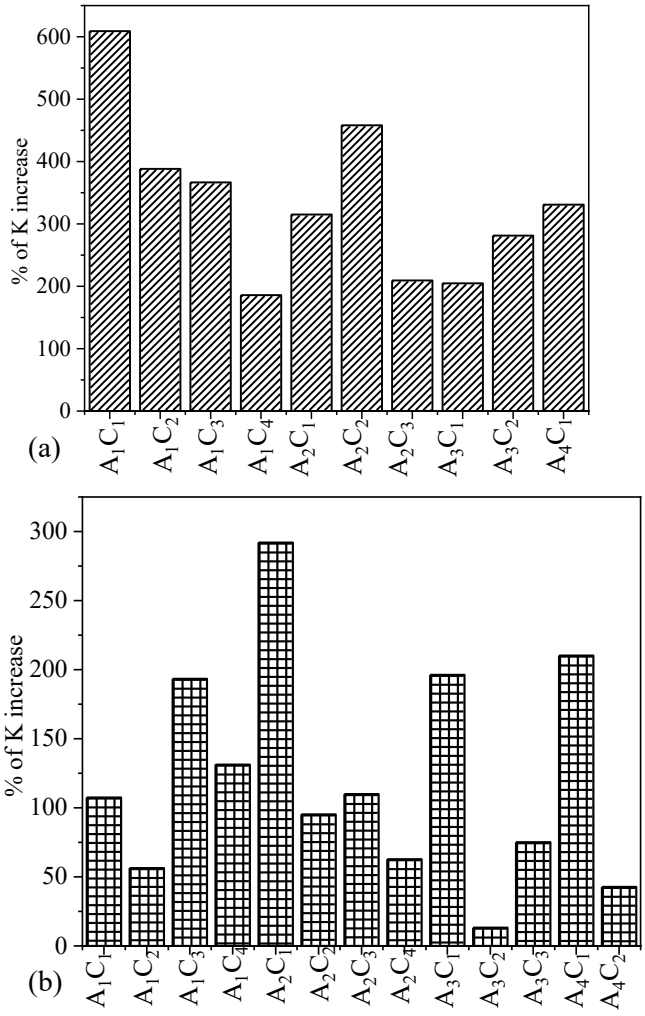

FIGURE 8: PERCENTAGE OF K (VISCOSITY AT 1.0 s^{-1} SHEAR RATE) INCREASE OF COMPOSITIONS HAVING (A) 1% TO-NFC COMPARED TO 0.01% TO-NFC AND (b) 0.5% TO-NFC COMPARED TO 0.005% TO-NFC.

3.4 Analysis of filament width after 3D printing

To analyze the effect of TO-NFC on the printability of various compositions having 0.005%, 0.5%, 0.01%, and 1.0% TO-NFC were considered to 3D print.

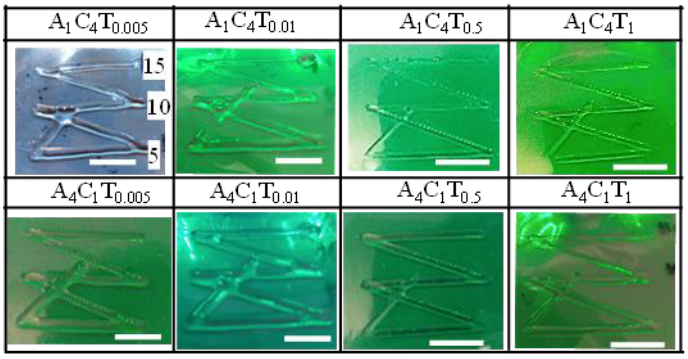

FIGURE 9: PERCENTAGE OF K (VISCOSITY AT 1.0 s^{-1} SHEAR RATE) INCREASE OF COMPOSITIONS HAVING (a) 1% TO-NFC COMPARED TO 0.01% TO-NFC AND (b) 0.5% TO-NFC COMPARED TO 0.005% TO-NFC.

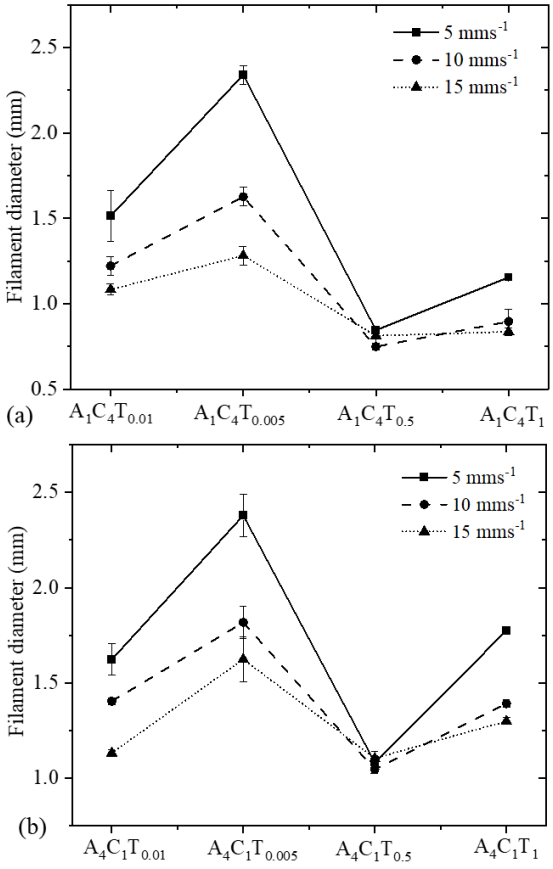

FIGURE 10: PERCENTAGE OF K (VISCOSITY AT 1.0 s^{-1} SHEAR RATE) INCREASE OF COMPOSITIONS HAVING (a) 1% TO-NFC COMPARED TO 0.01% TO-NFC AND (b) 0.5% TO-NFC COMPARED TO 0.005% TO-NFC.

Total eight compositions such as $A_1C_4T_{0.005}$, $A_1C_4T_{0.5}$, $A_1C_4T_{0.01}$, $A_1C_4T_1$, $A_4C_1T_{0.005}$, $A_4C_1T_{0.5}$, $A_4C_1T_{0.01}$, and $A_4C_1T_1$ were chosen to print them with three different print speeds such as 5, 10, and 15 mm/s as shown in Figure 9. The detail printing process and method to determine the shape fidelity were discussed in section 2.3. Our first observation was all compositions were 3D-printable and filaments preserved the shape. Filament diameters for each composition were determined as shown in Figure 10. Figures 9 and 10 depict that with increasing the percentage of TO-NFC, the filament geometry was better defined with reduced diameter. For an example the filament fabricated with the composition of $A_1C_1T_{0.005}$ at 10 mm/s showed 17% higher diameter than filament fabricated with the composition of $A_1C_1T_{0.01}$ because of its higher percentage of To-NFC. Therefore, the graph depicted in Figure 10 (a-b) showed a zigzag fashion based on its TO-NFC percentages. For any compositions, the filament width was reduced with increasing print speed. For an example, filament width for composition $A_1C_4T_{0.005}$ was reduced up to 21.2% for print speed of 10mms^{-1} and 30.5% for print speed of 15mms^{-1} compared to the filament width printed with 5mms^{-1}. Similar scenario was observed for other compositions as shown in Figure 10.

4. CONCLUSION

In this research, for a total of 46 compositions, rheological analysis was conducted to identify the effect of various percentage of TO-NFC on varying percent of alginate and CMC. To fabricate a large-scale functional tissue scaffold with appropriate hybrid hydrogel, this experimental analysis can help identify right material to ensure geometrical fidelity by controlling the filament width. In future, we will print filaments with all compositions, determine the filament width and explore analytical model enabling a relation between filament width and percentage of TO-NFC. The illustrated characterization techniques can direct the 3D bio-fabrication of the tailored anisotropic scaffolds, which will assist the fabrication of functional tissue in the future.

ACKNOWLEDGEMENTS

Research was supported by New Hampshire-EPSCoR through BioMade Award #1757371 from National Science Foundation and New Hampshire-INBRE through an Institutional Development Award (IDeA), P20GM103506, from the National Institute of General Medical Sciences of the NIH.

REFERENCES

[1] L. Ouyang, C. B. Highley, C. B. Rodell, W. Sun, and J. A. Burdick, "3D printing of shear-thinning hyaluronic acid hydrogels with secondary cross-linking," *ACS Biomaterials Science & Engineering,* vol. 2, no. 10, pp. 1743-1751, 2016.

[2] J. Malda *et al.*, "25th anniversary article: engineering hydrogels for biofabrication," *Advanced materials,* vol. 25, no. 36, pp. 5011-5028, 2013.
[3] F. J. O'brien, "Biomaterials & scaffolds for tissue engineering," *Materials today,* vol. 14, no. 3, pp. 88-95, 2011.
[4] H.-J. Kong, K. Y. Lee, and D. J. Mooney, "Decoupling the dependence of rheological/mechanical properties of hydrogels from solids concentration," *Polymer,* vol. 43, no. 23, pp. 6239-6246, 2002.
[5] A. B. Dababneh and I. T. Ozbolat, "Bioprinting technology: a current state-of-the-art review," *Journal of Manufacturing Science and Engineering,* vol. 136, no. 6, 2014.
[6] A. Schwab, R. Levato, M. D'Este, S. Piluso, D. Eglin, and J. Malda, "Printability and shape fidelity of bioinks in 3D bioprinting," *Chemical reviews,* vol. 120, no. 19, pp. 11028-11055, 2020.
[7] T. Xu, J. Jin, C. Gregory, J. J. Hickman, and T. Boland, "Inkjet printing of viable mammalian cells," *Biomaterials,* vol. 26, no. 1, pp. 93-99, 2005.
[8] D. Wu and C. Xu, "Predictive modeling of droplet formation processes in inkjet-based bioprinting," *Journal of Manufacturing Science and Engineering,* vol. 140, no. 10, 2018.
[9] J. H. Chung *et al.*, "Bio-ink properties and printability for extrusion printing living cells," *Biomaterials Science,* vol. 1, no. 7, pp. 763-773, 2013.
[10] Z. M. Jessop *et al.*, "Printability of pulp derived crystal, fibril and blend nanocellulose-alginate bioinks for extrusion 3D bioprinting," *Biofabrication,* vol. 11, no. 4, p. 045006, 2019/07/08 2019, doi: 10.1088/1758-5090/ab0631.
[11] R. Devillard *et al.*, "Cell patterning by laser-assisted bioprinting," in *Methods in cell biology*, vol. 119: Elsevier, 2014, pp. 159-174.
[12] B. Guillotin *et al.*, "Laser assisted bioprinting of engineered tissue with high cell density and microscale organization," *Biomaterials,* vol. 31, no. 28, pp. 7250-7256, 2010.
[13] M. Habib and B. Khoda, "Fiber Filled Hybrid Hydrogel for Bio-Manufacturing," *Journal of Manufacturing Science and Engineering,* pp. 1-38, 2020.
[14] M. Di Giuseppe *et al.*, "Mechanical behaviour of alginate-gelatin hydrogels for 3D bioprinting," *Journal of the mechanical behavior of biomedical materials,* vol. 79, pp. 150-157, 2018.
[15] T. Agarwal, S. G. H. Narayana, K. Pal, K. Pramanik, S. Giri, and I. Banerjee, "Calcium alginate-carboxymethyl cellulose beads for colon-targeted drug delivery," *International journal of biological macromolecules,* vol. 75, pp. 409-417, 2015.
[16] Q. Garrett *et al.*, "Carboxymethylcellulose binds to human corneal epithelial cells and is a modulator of corneal epithelial wound healing," *Investigative ophthalmology & visual science,* vol. 48, no. 4, pp. 1559-1567, 2007.
[17] L. K. Narayanan, P. Huebner, M. B. Fisher, J. T. Spang, B. Starly, and R. A. Shirwaiker, "3D-bioprinting of polylactic acid (PLA) nanofiber–alginate hydrogel bioink containing human adipose-derived stem cells," *ACS Biomaterials Science & Engineering,* vol. 2, no. 10, pp. 1732-1742, 2016.
[18] D. Nguyen *et al.*, "Cartilage tissue engineering by the 3D bioprinting of iPS cells in a nanocellulose/alginate bioink," *Scientific reports,* vol. 7, no. 1, p. 658, 2017.
[19] V. C. Li, A. Mulyadi, C. K. Dunn, Y. Deng, and H. J. Qi, "Direct Ink Write 3D Printed Cellulose Nanofiber Aerogel Structures with Highly Deformable, Shape Recoverable, and Functionalizable Properties," *ACS Sustainable Chemistry & Engineering,* vol. 6, no. 2, pp. 2011-2022, 2018.
[20] L. Ouyang, R. Yao, Y. Zhao, and W. Sun, "Effect of bioink properties on printability and cell viability for 3D bioplotting of embryonic stem cells," *Biofabrication,* vol. 8, no. 3, p. 035020, 2016.
[21] A. Blaeser, D. F. Duarte Campos, U. Puster, W. Richtering, M. M. Stevens, and H. Fischer, "Controlling shear stress in 3D bioprinting is a key factor to balance printing resolution and stem cell integrity," *Advanced healthcare materials,* vol. 5, no. 3, pp. 326-333, 2016.
[22] D. Therriault, S. R. White, and J. A. Lewis, "Rheological behavior of fugitive organic inks for direct-write assembly," *Applied Rheology,* vol. 17, no. 1, pp. 10112-11411, 2007.
[23] R. Schwartz, M. Malpica, G. L. Thompson, and A. K. Miri, "Cell encapsulation in gelatin bioink impairs 3D bioprinting resolution," *Journal of the mechanical behavior of biomedical materials,* vol. 103, p. 103524, 2020.
[24] R. S. Kumar V, Cutkosky M, Dutta D, " Representation and processing heterogeneous objects for solid freeform fabrication," ed. Sixth IFIP WG 5.2 International Workshop on Geometric Modelling: Fundamentals and Applications, Tokyo, Japan, The University of Tokyo, 1998.